Oct 18th, 12:00 AM

Doubly Corrugated Barrel Cold-formed Steel Shells

G. L. Pierce

W. D. Siddall

George Adbel-Sayed

DOUBLY CORRUGATED BARREL COLD-FORMED STEEL SHELLS

by

G. Abdel-Sayed[1], G.L. Pierce[2], and W.D. Siddall[3]

(1) Professor of Civil Engineering, University of Windsor, Windsor, Ontario.

(2) Research Officer, Industrial Services Division, Saskatchewan Research Council, Saskatoon, Saskatchewan.

(3) Manager, Technical Services and Engineering, Fairford Industries Ltd., Moose Jaw, Saskatchewan.

INTRODUCTION

The present paper deals with the analysis of cold-formed steel cylindrical barrel (quonset) buildings, Fig. 1. An estimated 10,000 buildings of this type are erected each year in North America with spans ranging from 25 ft (7.62 m) to 100 ft (30.48 m). The majority of these buildings are used for warehouses, grain storages, and farm utility shelters. They are also increasingly being used for high human occupancy buildings such as community and recreational facilities.

The barrel buildings are usually constructed from deep U-shaped cold-formed steel panels (Fig. 2). The desired building curvature is obtained by developing small cross-corrugations in the lower part of the section. These cross-corrugations have significant effect on the performance and rigidity of the panel. They improve its local buckling characteristics and reduce its bending and axial rigidity in the curved direction. Under loading, the stresses and deformations of the panel are governed by the depth of the cross-corrugation which is related to the radius of curvature of the building.

Until recently, information concerning the structural performance of these buildings was very sketchy. The present paper establishes and discusses procedures to calculate the mechanical properties of the steel panels, as well as to analyse the building. The structure may be treated as an arch or as a shell, depending on the length to span ratio, the presence of longitudinal stiffeners, and the loading and support conditions.

CROSS-CORRUGATION

The U-shaped cold-formed steel panels are usually made with width 24 in (600 mm) and a depth of 8 in (200 mm). The depth of the cross-corrugation, 2f, Fig. 2c, is related to the radius of curvature, R, of the building. It

is variable over the cross-section and is found to be governed by the formula:

$$f = g\sqrt{\frac{e}{8R}} \tag{1}$$

in which g = half pitch of corrugation; and e = the distance down from the top of the overall U-shaped section at which the depth of corrugation is being calculated, Fig. 2b, c.

Considering the cross-corrugation to have the form of a sine wave, the relation between the local forces and strains in the ϕ-direction is governed by the local axial rigidity, d_ϕ (1):

$$d_\phi = \frac{Et}{6(1-\mu^2)}\left(\frac{t}{f}\right)^2 \tag{2}$$

in which t = metal thickness; E = modulus of elasticity; and μ = Poisson's ratio.

The half depth of cross-corrugation, f, varies from a maximum value at the bottom of the U-section to zero near the top. Eq. 2 is modified to be valid for the entire range including the zone with very shallow depth of corrugation. This is accomplished by adding the effect of tensile strains to the bending deformation which were the only consideration given when developing Eq. 2. The modified equation takes the form:

$$d_\phi = \frac{Et}{(1-\mu^2)\left(6\frac{f^2}{t^2} + 1\right)} \tag{3}$$

Equations 2 and 3 are valid within the elastic range of stresses and considering only small deformations. In order to account for large deformations and for the elastic-plastic range of stresses, the method of finite element method is applied.

A finite element model of 180° of the cross-corrugation sine wave profile is constructed of sixteen two-dimensional isoparametric solid elements (5). A specified displacement in the ϕ-direction is applied and the resulting forces are used to calculate the local rigidity. The displacement on the model is increased causing part of the model to experience plastic deformation. Also, the change in geometry is included in the analysis to account for the flattening (under tension) or increased depth of corrugation (under compression).

The analytical results were compared with experimental results reported in reference (3). The comparison is outlined in Table 1 which shows good agreement between the analysis and the experimental data.

Using the actual dimension of a cross-corrugation (g = 1 in (25.4 mm), t = 0.0359 in (0.91 mm)), the finite element analyses were conducted to determine the local axial rigidity, d_ϕ, for varying values of corrugation depth. Table 2 compares the finite element results within the elastic range with those obtained from Eqs. 2 and 3.

PANEL PROPERTIES

The sectional properties of the U-shaped profile are calculated by dividing it into a number of small segments. Using Eq. 1 together with equations 2, 3 or the finite element results, the local axial rigidity of each segment is calculated. The contribution of each segment is integrated to determine the bending and axial rigidity of the panel as well as the location of its neutral axis. Also, the bending and axial rigidities of the panel are calculated in the lateral direction using a similar approach. The rigidity of equivalent orthotropic material is calculated as the average rigidity per unit width. Table 3 shows the analytically obtained results and those obtained experimentally (8) for three different panels.

ULTIMATE LOAD CARRYING CAPACITY

The ultimate load carrying capacities are calculated for the panels subjected to combined bending and axial forces. The panel failure is assumed to occur due to compressive yield in the zone of flat or shallow cross-corrugation. This assumption is applied since panel tests showed that yielding in the zone of deep corrugation constitutes no failure criteria and takes place well before the ultimate load carrying capacity is reached in the U-section (11). Figure 3 shows an example comparing the theoretical results with those obtained experimentally.

METHODS OF ANALYSIS

The building consists of a series of arches bolted together. Plane end walls usually complete the basic structure allowing it to perform as a cylindrical shell supported along its four edges. However, with the increase in the ratio of length to span of the building, its middle portion reaches a state in which it is not affected by the end walls and acts as an arch. Therefore, both the arch and shell analysis are presented here.

ARCH ANALYSIS

The arch is considered as a polygon composed of straight elements and is treated as a statically indeterminate frame with loading applied at the joints (Fig. 4). The relation between the applied loading Q and the displacement vector D is governed by the stiffness matrix K:

$$\{Q\} = [K]\{D\} \tag{4}$$

The stiffness matrix K is generated by assembling the stiffness matrices k_i of the individual elements. Because of the flexibility of the arch, its analysis is conducted taking into consideration the nonlinear terms in the

strain-displacement equations which leads the stiffness matrix of each element to be expressed as:

$$k_i = k_{Ei} + k_{Gi} \tag{5}$$

in which k_{Ei} = the linear elastic stiffness matrix of a beam element and k_{Gi} = the geometric stiffness matrix which is dependent on the geometry and the internal forces in the element (9):

$$k_{Ei} = \frac{EI}{\ell^3} \begin{bmatrix} \frac{A\ell^2}{I} & 0 & 0 & -\frac{A\ell^2}{I} & 0 & 0 \\ 0 & 12 & 6\ell & 0 & -12 & 6\ell \\ 0 & 6\ell & 4\ell^2 & 0 & -6\ell & 2\ell \\ -\frac{A\ell^2}{I} & 0 & 0 & \frac{A\ell^2}{I} & 0 & 0 \\ 0 & -12 & -6\ell & 0 & 12 & -6\ell \\ 0 & 6\ell & 2\ell^2 & 0 & -6\ell & 4\ell^2 \end{bmatrix} \tag{6a}$$

and

$$k_{Gi} = \frac{F}{\ell} \begin{bmatrix} 0 & 0 & 0 & 0 & 0 & 0 \\ 0 & \frac{6}{5} & \frac{\ell}{10} & 0 & -\frac{6}{5} & \frac{\ell}{10} \\ 0 & \frac{\ell}{10} & \frac{2\ell^2}{15} & 0 & -\frac{\ell}{10} & -\frac{\ell^2}{30} \\ 0 & 0 & 0 & 0 & 0 & 0 \\ 0 & -\frac{6}{5} & -\frac{\ell}{10} & 0 & \frac{6}{5} & -\frac{\ell}{10} \\ 0 & \frac{\ell}{10} & -\frac{\ell^2}{30} & 0 & -\frac{\ell}{10} & \frac{2}{15}\ell^2 \end{bmatrix} \tag{6b}$$

in which E = modulus of elasticity; A and I = area and moment of inertia of the section, respectively; ℓ = length of the member; and F = axial force in the member.

Because of the presence of nonlinear terms, an iterative procedure is required to obtain solutions to the governing matrix equations. A computer program is written, in which the problem is treated as a sequence of linear steps. Each step represents a load increment, followed by modifying the geometric configuration of the arch, as well as establishing the axial force, F, in each member.

As a by-product of this large-deflection analysis, the buckling load is determined when the stiffness matrix becomes a non-positive definite.

The analytical results were compared with experimental results obtained from testing model arches (10). The dimensions and loading system applied to one of these arches are shown in Fig. 5. A comparison between the analysis and the experimental results is presented in Fig. 6. The analytically predicted behaviour of the arch reasonably agrees with the experimentally obtained results. The buckling load is found analytically to be 440 lbs., while complete collapse of the model arch occurred at 459 lbs.

The arches are supported by concrete footing either through base plates, Fig. 7a, or by being embedded in the concrete, Fig. 7b. The effect of the support conditions is examined by comparing the behaviour of arches with two fully fixed or two hinged supports. Figure 8 shows the bending moment diagrams considering the two cases of supports for an arch (R = 310 in (79 m), ϕ_c = 75.1°, t = 0.03 in (0.76 mm)) subjected to uniform load over the horizontal projection. Fixing the supports leads to a reduction of 60% in the positive moment at the crown and of 48% in the negative moments at the sides. Additional positive moment is developed at the supports with a magnitude higher than the original

moment at the crown. However, the actual behaviour of the arch depends on the degree of fixation, and the actual bending moment diagram falls somewhere between the two given diagrams (11). Furthermore, the fixed arch shows higher rigidity when compared with the two hinged arches, Fig. 9, and its buckling load is increased to almost twice that of the two hinged arch.

SHELL ANALYSIS

The shell is analyzed using the theory of orthotropic cylindrical shells. The differential equations governing the behaviour of the shell are formulated taking into consideration the special character of the panels in which the rigidities in the curved direction are considerably higher than those in the longitudinal direction. The three governing simultaneous equations are given in the displacement components u, v and w in the x-, ϕ- and z-directions, respectively (2):

$$D_x R \frac{\partial^2 u}{\partial x^2} + D_{x\phi}\left(\frac{1}{R} \frac{\partial^2 u}{\partial \phi^2} + \frac{\partial^2 v}{\partial x \partial \phi} \right) + p_x R = 0 \qquad (7a)$$

$$D_\phi \left(\frac{\partial^2 v}{\partial \phi^2} - \frac{\partial w}{\partial \phi} \right) + D_{x\phi}\left(R \frac{\partial^2 u}{\partial x \partial \phi} + R^2 \frac{\partial^2 v}{\partial x^2} \right) + \frac{3B_{x\phi}}{2} \left(\frac{\partial^2 v}{\partial x^2} + \frac{\partial^3 w}{\partial x^2 \partial \phi} \right) + R^2 p_\phi = 0 \qquad (7b)$$

$$\frac{B_\phi}{R^2}\left(- \frac{\partial^4 w}{\partial \phi^4} - \frac{2\partial^2 w}{\partial \phi^2} - w \right) + D_\phi \left(\frac{\partial v}{\partial \phi} - w \right) - 2B_{x\phi} \frac{\partial^4 w}{\partial x^2 \partial \phi^2} - B_x R^2 \frac{\partial^4 w}{\partial x^4} + R^2 p_z = 0 \qquad (7c)$$

in which p_x, p_ϕ and p_z are the external loading per unit area of middle surface acting in the x, y and z directions, respectively.

The application of the theory of orthotropic shells and the above equations were experimentally proven to be adequate in determining the behaviour of model shells made of corrugated steel sheets in which similar wide differences exist between the rigidities in the two principal directions (1, 2).

The effective axial rigidity, D_ϕ, and bending rigidity, B_ϕ, are calculated as the average rigidities per unit width of the cross-section. In a similar manner, the axial rigidities, D_x, and bending rigidity, B_x, are calculated in the lateral direction of the panel (Table 3). The shear rigidity, $D_{x\phi}$, is calculated as (1):

$$D_{x\phi} = \rho \frac{Et}{2(1+\mu)} \frac{c}{d} \tag{8}$$

in which c and d = horizontal projection and developed length of the panel's section, respectively; ρ = a reduction factor to account for the effect of slip at the connection between sheets and between the sheets and end walls. The torsional rigidity is expressed as:

$$B_{x\phi} = \alpha\sqrt{B_x B_\phi} \tag{9}$$

in which α = a factor which is expected to be less than one for open section (4).

In order to examine the effect of the factor α on the analytical results, the shell outlined in Table 4 is analyzed considering different values for α ranging from 0.2 to 1.0. The maximum deflection, Δ, bending moment, M_ϕ, and axial force, N_x, obtained for a uniform load of one psf over the horizontal projection are as follows:

α	Δ in	M_ϕ lb. in/in	N_x lb/in
0.2	0.0658	12.87	2.091
0.6	0.0660	12.89	2.093
1.0	0.0660	12.91	2.094

It is noticed that the magnitude of α has practically no effect on the results of the shell analysis which can therefore be conducted with a rough approximate for α.

Numerical analysis shows that unless the shell is very short, the shell action can hardly be observed in the case of a building with no longitudinal stiffeners. This is due to the very low axial rigidity, D_x, in the longitudinal direction. This rigidity can be easily increased by providing longitudinal stiffeners and assuming their effect to be uniform over the arch length. The axial rigidity is calculated as:

$$D_x = \frac{A_s E}{s} \beta \tag{10}$$

in which A_s = cross-sectional area of stiffener, E = modulus of elasticity; s = spacing between stiffeners; and β = a reduction factor to account for the non-uniform distribution of the forces in the longitudinal direction. Table 4 shows a comparison between the deflections and internal force components when considering different numbers of stiffeners. An assumed value of $\beta = 0.4$ was found to lead to analytical results of reasonable agreement with those obtained experimentally from full scale tests with the length of shell equal to its span (11). For longer shells, similar comparisons show a trend in which β should be increased with the increase in the ratio of length to span (11).

In addition to the cases of loading examined in reference (2), a general case of gravity load with variation in the arch direction is considered here. This loading is expressed in the form of a single fourier series:

$$p = \sum_{n=1}^{\alpha} p_n \sin \frac{n\pi}{2\phi_e} \sin \frac{\pi}{L} x \tag{11}$$

in which ϕ = the angle measured from support and L = length of the shell. The loading is analysed in the radial and tangential direction (p_z and p_ϕ, respectively). A particular solution is obtained by satisfying the governing equations and is superimposed to a homogeneous solution to satisfy the boundary

conditions along the longitudinal edges. Solutions are obtained for both cases of shells supported along fixed and hinged edges (Table 4).

OBSERVATIONS

1. Buildings with large length to span ratio or without adequate longitudinal stiffeners may be analyzed as cylindrical arches. These arches are flexible and their nonlinear behaviour and stability are important design criteria. Figure 10 shows the behaviour of an example two hinged arch with 100 ft. span subjected to uniform load on horizontal projection. The critical buckling load is found to be 38 psi and the moment magnifying factor is 1.18 at $P = 0.5\ P_{cr}$ and 1.31 at $P = 0.75\ P_{cr}$.

2. The stability conditions of the building are significantly improved when adding longitudinal stiffeners. Figure 11 shows a sharp increase in the buckling load even with the least number of stiffeners. Therefore, with the existence of end walls and the minimum requirements for shell action, buckling ceases to be a major design criteria of the building.

3. Figure 12 shows the variation of maximum moment, M_ϕ, with different numbers of stiffeners. The stiffeners have a significant effect especially for short shells (L/S = 1). This effect is reduced with the increase of the length to span ratio.

4. Under uniform loading, the building behaves more like an arch when the length becomes twice the span. However, the shell action remains significant for such a long shell when subjected to non-symmetric loading. This can be observed in Fig. 13, which shows the bending moment diagrams obtained by analyzing the building as an arch and as a shell with lengths of 50 and 100 ft.

CONCLUSION

The doubly corrugated barrel cold-formed steel shells are analyzed using the orthotropic cylindrical shell theory. The mechanical properties of the shell walls (average properties of the steel panels) are calculated analytically and verified experimentally. The building may behave as a plane arch or as a three-dimensional shell, depending on its length to span ratio, longitudinal stiffeners, and on the loading and support conditions.

APPENDIX I - REFERENCES

1. Abdel-Sayed, G., "Critical Shear Loading of Curved Panels of Corrugated Sheets", Journal of Engineering Mechanics Division, ASCE, December 1970, pp. 895-912.

2. El-Atrouzy, M. and Abdel-Sayed, G., "Prebuckling Analysis of Orthotropic Barrel-Shells", Journal of the Structural Division, ASCE, November 1978, pp. 1775-1786.

3. El-Atrouzy, M.N., "Structural Properties of Corrugated Sheets Used in Cylindrical Shells", M.Sc. Thesis, University of Windsor, Windsor, Ontario, 1969.

4. Hawranek, A. and Steinhardt, O., "Theorie und Berechnung der Stahlbruecken", Springler-Verlag, Berlin, 1958.

5. Kohnke, P.C., "Ansys - Engineering System - Theoretical Manual", Nov. 1, 1977, Swanson Analysis System Inc., Houston, Pennsylvania.

6. Marzouk, O. and Abdel-Sayed, G., "Linear Theory of Orthotropic Cylindrical Shells", Journal of the Structural Division, ASCE, November 1973, pp. 2287-2306.

7. Marzouk, O. and Abdel-Sayed, G., "Stability of Half-Barrel Orthotropic Shells", Journal of the Structural Division, ASCE, July 1975, pp. 1517-1530.

8. Pierce, G., "Design Research Project on Quonset Buildings of the Type Produced by Fairford Industries in Moose Jaw, Saskatchewan", Industrial Service Division, Saskatchewan Research Council, Saskatoon, 1976.

9. Przemieniecki, J.S., Theory of Matrix Structural Analysis , McGraw-Hill, New York, 1968.

10. Schepers, A., "Analysis and Stability of Circular Arches", 4th Year Thesis, Department of Civil Engineering, University of Windsor, 1976.

11. Siddal, W., Pierce, G., and Abdel-Sayed, G., "Full Scale Testing and Analysis of Circular Arch Skin-Supported Steel Shell Buildings", Proc. of the Annual Conference of the CSCE, Winnipeg, May 1980.

APPENDIX II - NOTATION

The following symbols are used in this paper:

A = effective cross-sectional area of the arch

A_s = cross-sectional area of stiffener

B_x, B_ϕ = bending rigidity in the xz- and ϕz-planes, respectively

$B_{x\phi}$ = torsional rigidity

c = horizontal projection of the section

d = developed length of the section

d_ϕ = local axial rigidity of cross-corrugated zone

D = displacement vector

D_x, D_ϕ = axial rigidity in the x- and ϕ-directions, respectively

$D_{x\phi}$ = shear rigidity in the $x\phi$-plane

e = distance measured down from the top of the U-shaped section

E = modulus of elasticity

f = half depth of cross-corrugation

F = axial force in arch component

g = half pitch of arch component

I = effective moment of inertia of the panel

k_i = element stiffness matrix

k_{Ei} = linear elastic stiffness matrix

k_{Gi} = geometric stiffness matrix

K = general stiffness matrix

ℓ = length of polygon member

L = length of the barrel shell

M_x, M_ϕ = bending moment in the x- and ϕ-directions, respectively

$M_{x\phi}$ = torsional moment

N_x, N_ϕ = axial force in the x- and ϕ-directions, respectively

$N_{x\phi}$ = shear force in $x\phi$-plane

Q = loading vector

R = radius of curvature of the shell

s = spacing between stiffeners

S = span of the shell

t = average thickness of material

u, v, w = displacement in the x-, ϕ- and z-directions, respectively

α, β = factors determining the torsional and axial rigidities, respectively

ρ = reduction factor for shear rigidity

μ = Poisson's ratio

Table 1 - Comparison Between Experimental and Analytical Results for Corrugated Sheets Under Tension, g = 5.32 in (135.1 mm), f = 0.25 in (6.35 mm), t = 0.035 in (0.91 mm)

Force, lb/in	Tensile Strain		
	0.00075	0.017	0.0717
Finite Element Method	2.7	62.2	159.8
Experiment (3)	3.2	71.4	158.0

1 in = 25.4 mm, 1 lb = 4.448 N.

Table 2 - Calculated and Test Results for the Local Axial Rigidity, d_ϕ, Within the Elastic Range

Pitch, g in	5.32	1.0	1.0	1.0	1.0	1.0
Thickness, t in	0.0359	0.0359	0.0359	0.0359	0.0359	0.0359
Half Depth of Corrugation, f in	0.26	0.10	0.051	0.01	0.004	0
d_ϕ lb/in x 10^6						
Finite Element	0.004	0.024	0.090	0.807	1.10	1.18
Equation 2	0.004	0.023	0.097	2.510	15.8	∞
Equation 3	0.004	0.024	0.090	0.804	1.10	1.18
Experimental	0.004					

Table 3 - The Mechanical Properties of Equivalent Orthotropic Shell

Building Radius R in.	Metal Thickness t in.	Distance of Centroid from top of U $\bar{c}$, in.		Rigidity in ϕ-direction			Rigidity in x-direction		
				B_ϕ, lb. in/in		D_ϕ, lb/in	B_x, lb. in/in		D_x lb/in
		Anal.	Exp.	Anal.	Exp.	Anal.	Anal.	Exp.	Anal.
250	0.030	1.20	1.10	1.7×10^6	1.54×10^6	0.36×10^6	904	853	150
416	0.036	1.80	1.90	3.5×10^6	3.8×10^6	0.58×10^6	742	739	109
738	0.048	2.60	2.80	8.5×10^6	7.9×10^6	1.15×10^6	652	770	62

Table 4a — Deflection and Buckling Loads of a Cylindrical Building

t = 0.03 in,

Radius, R = 310 in,

ϕ_e = 75.1°

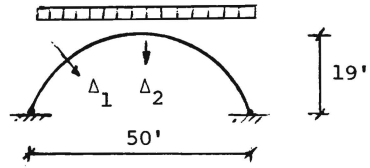

			Length of Shell					
			50 ft			76 ft		
		D_x	Δ_1	Δ_2	P_{cr}	Δ_1	Δ_2	P_{cr}
Hinged Longitudinal Edges	Arch Analysis	0.0	0.151	0.306	40	0.151	0.306	40
	Construction stiffeners	6400	0.083	0.139	197	0.101	0.291	142
	2 stiffeners	23200	0.042	0.066	229			
	3 stiffeners	39011	0.031	0.049	269	0.082	0.134	197
	5 stiffeners	46000	0.028	0.044	275	0.076	0.123	204
	9 stiffeners	78020	0.020	0.033	292	0.061	0.095	223
Fixed Longitudinal Edges	Arch Analysis	0.0	0.063	0.113	90	0.063	0.113	90
	Construction stiffeners	6400	0.051	0.109				
	2 stiffeners	23200	0.035	0.060		0.054	0.130	
	3 stiffeners	39011	0.027	0.047		0.052	0.104	
	5 stiffeners	46000	0.025	0.043		0.050	0.097	
	9 stiffeners	78020	0.019	0.034		0.045	0.079	

Table 4b - Maximum Bending Moments and Axial Forces in a Cylindrical Building

$t = 0.03$ in,

$R = 310$ in,

$\phi_e = 75.1°$

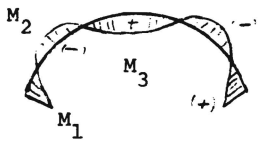

		Length of Shell							
		50 ft				76 ft			
		M_1	M_2	M_3	N_x	M_1	M_2	M_3	N_x
Hinged Longitudinal Edges	Arch Analysis	0	48.29	35.60	0	0	48.29	35.60	0
	Construction stiffeners	0	25.86	22.18	1.04	0	41.53	36.41	0
	2 stiffeners	0	12.89	11.03	2.09				
	3 stiffeners	0	9.44	8.03	2.42	0	25.31	21.67	0
	5 stiffeners	0	8.48	7.18	2.52	0	23.42	20.03	0
	9 stiffeners	0	6.39	5.28	2.78	0	18.51	15.79	0
Fixed Longitudinal Edges	Arch Analysis	42.09	23.50	21.60	0	42.09	23.50	21.60	0
	Construction stiffeners	44.64	20.86	19.12	0.36				
	2 stiffeners	28.74	12.93	11.73	1.44	48.63	23.26	21.39	0.215
	3 stiffeners	22.56	10.13	9.10	1.88	44.51	20.52	18.78	0.941
	5 stiffeners	20.69	9.29	8.30	2.03	42.71	19.52	17.84	1.238
	9 stiffeners	16.39	7.32	6.37	2.40	37.13	16.70	15.18	2.149

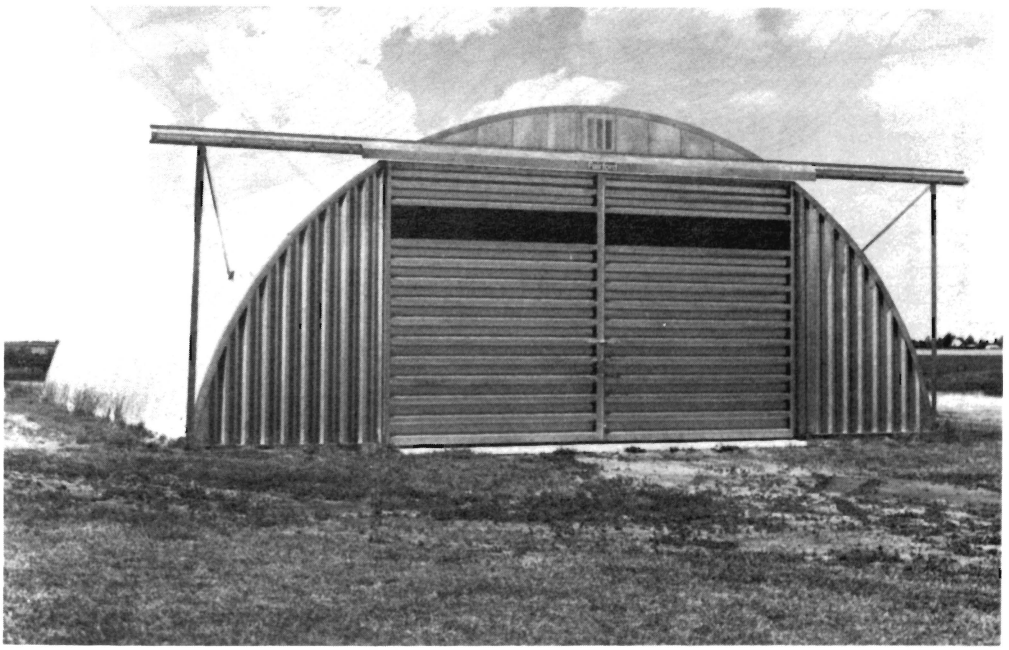

Fig. 1 Barrel "Quonset" Building

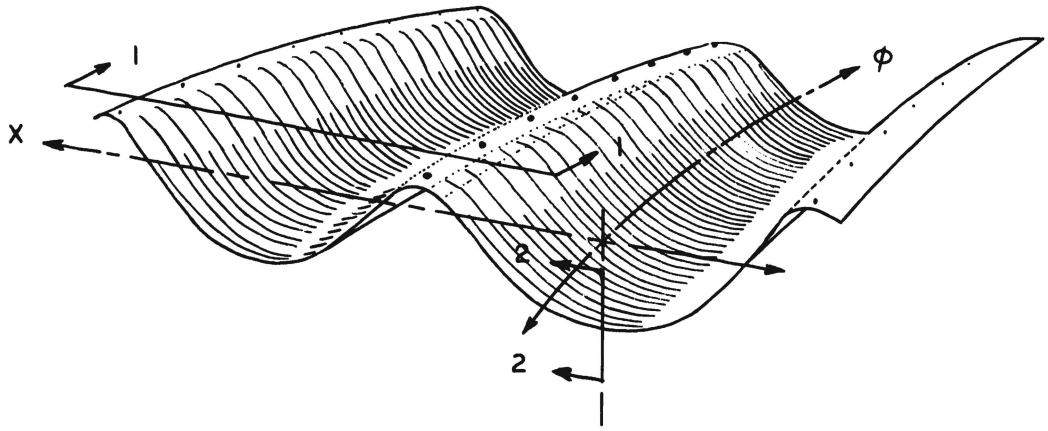

a) General Layout and Coordinates

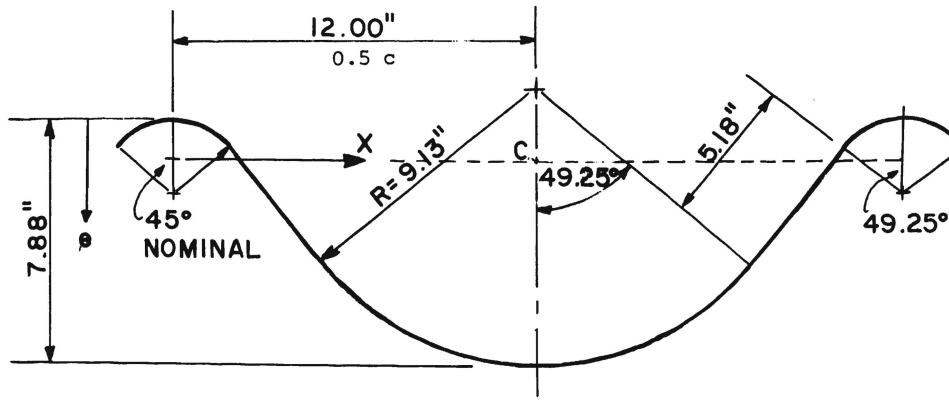

b) SECTION 1-1

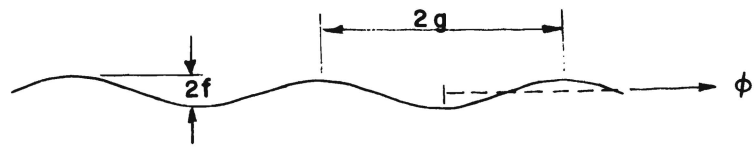

c) SECTION 2-2

Fig. 2 U-Shaped Cold-Formed Steel Curved Panels

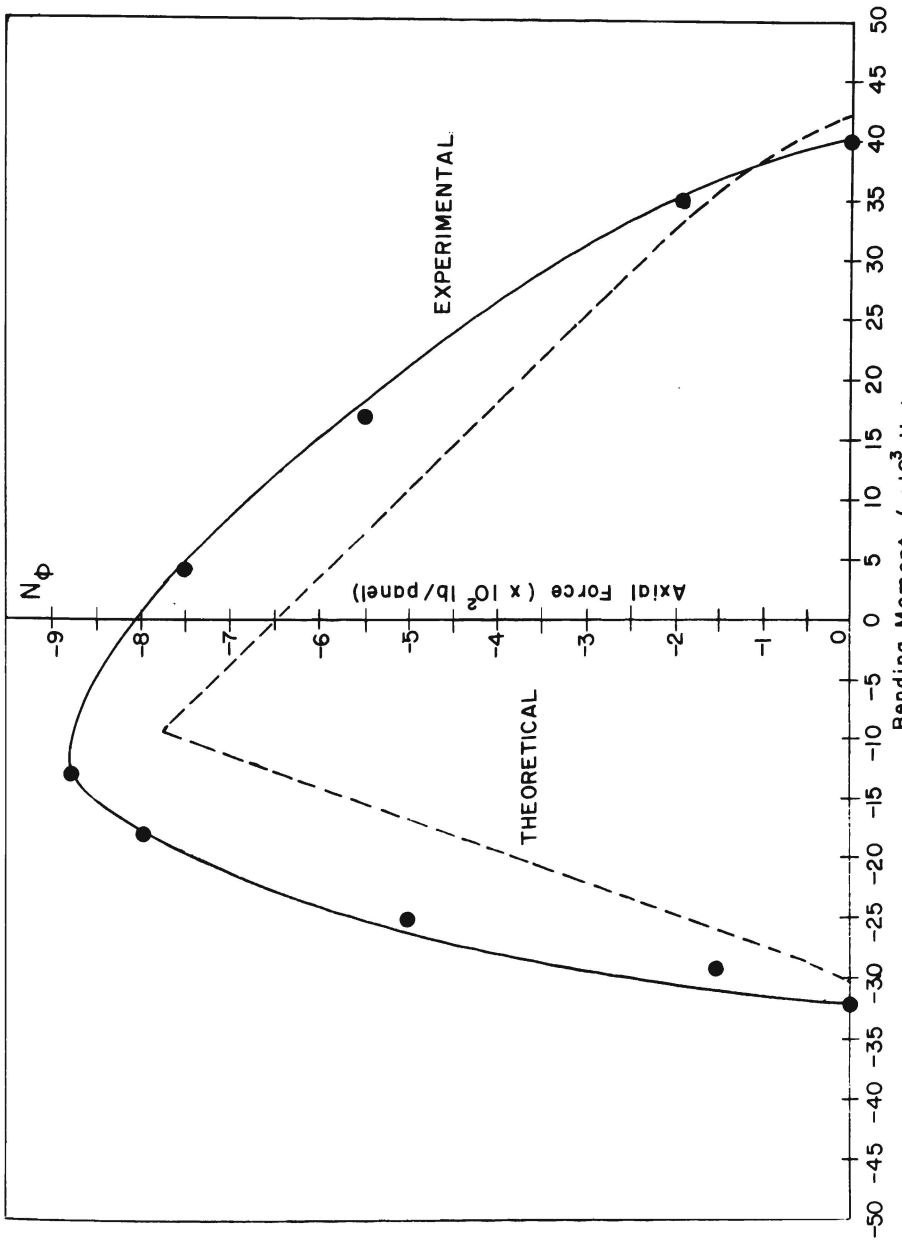

Fig. 3 Interaction Diagram, Ultimate Bending Moment, M_ϕ, vs. Axial Force, N_ϕ
(Panel of a building with radius R = 310 in, (79 m), t = 0.03 in (0.76 mm), Fig. 2)

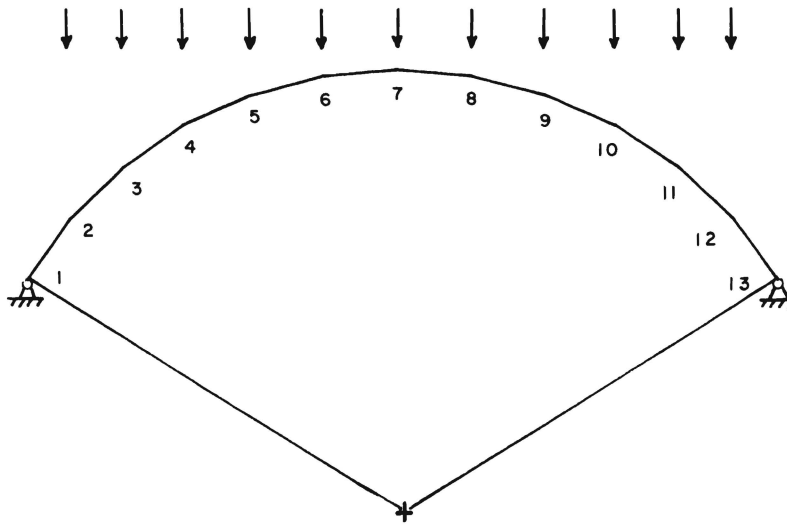

Fig. 4 Circular Arch Modeled as a Polygon

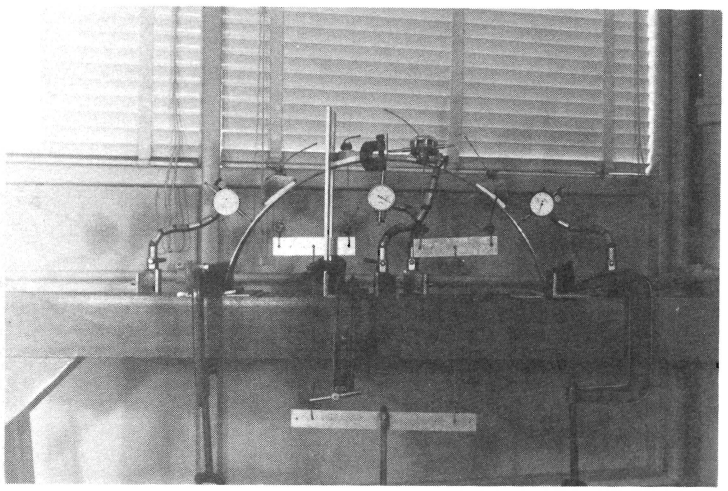

Fig. 5a Loading System on Mondel Arch
R = 13.2 in, $\phi_c = 80°$,
EI = 9440 Kip.in^2, EA = 7250 Kips

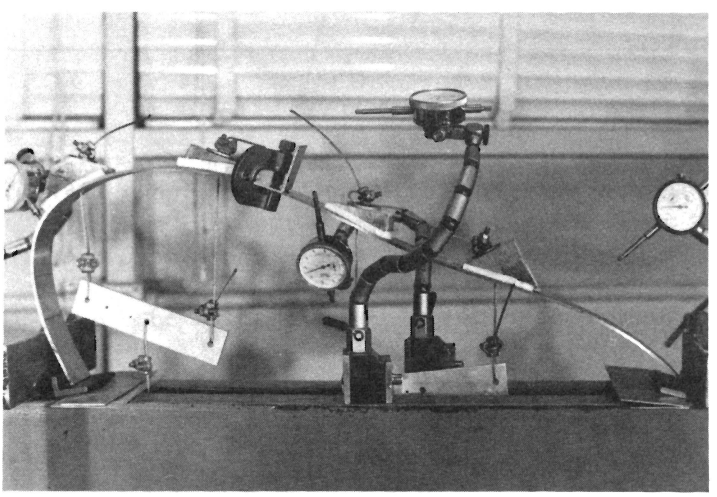

Fig. 5b Buckling Failure of Tested Arch
(Non-symmetric buckling mode)

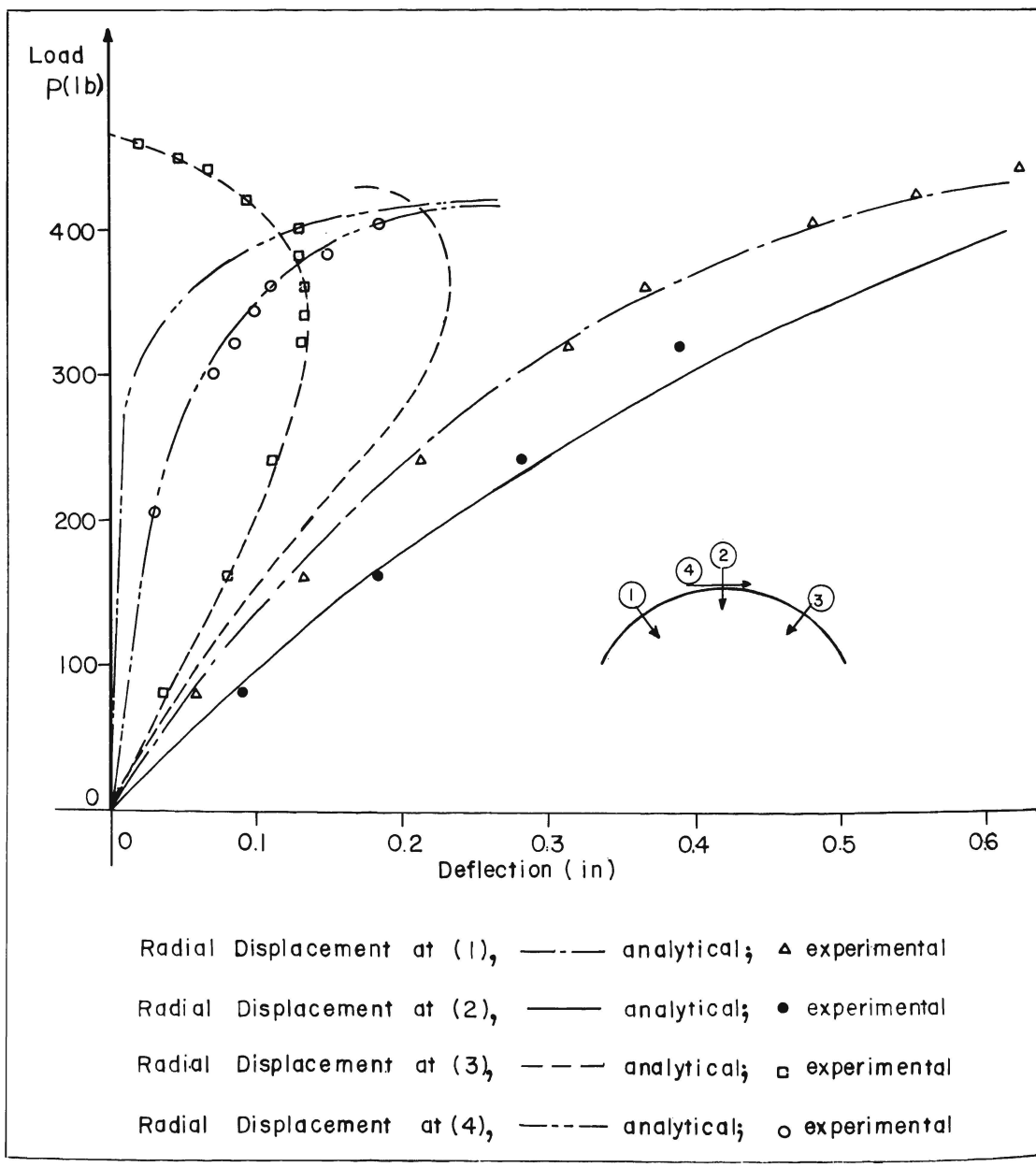

Fig. 6 Comparison Between Experimental and Analytical Results for Model Arch

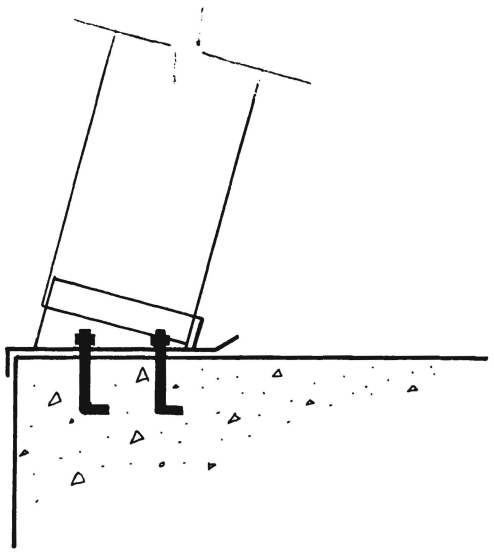

Fig. 7a Base Plate for Arch Support

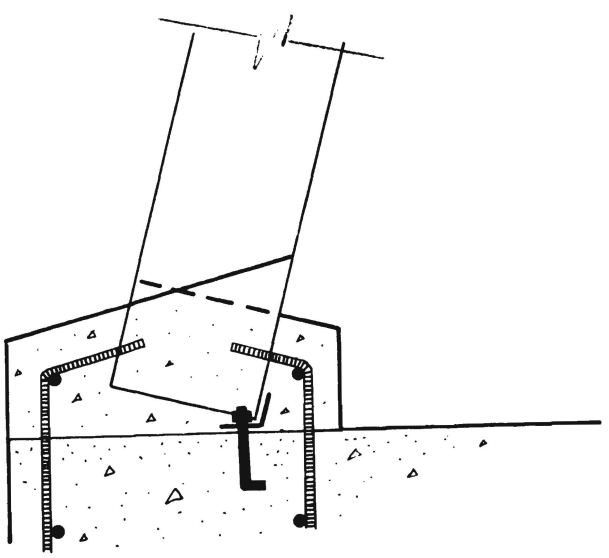

Fig. 7b Arch Base Embedded in Concrete

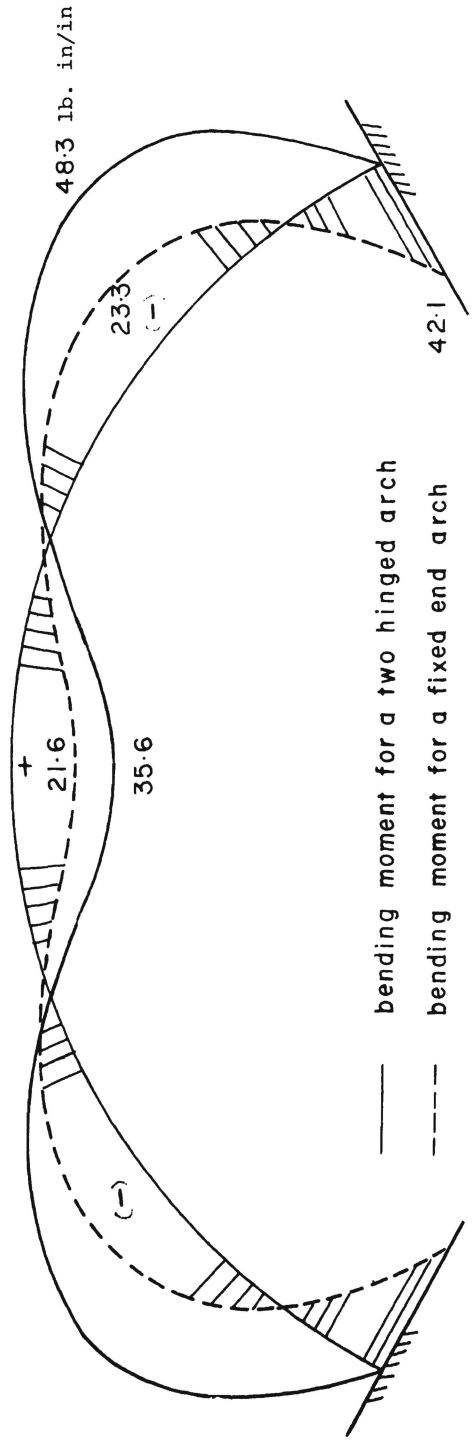

Fig. 8 Bending Moment Diagram for Arch Considering Supports to be Fully Fixed or Hinged

[S = 50 ft (15.24 m), R = 310 in (79 m), ϕ_e = 75.1°, t = 0.03 in (0.76 mm)]

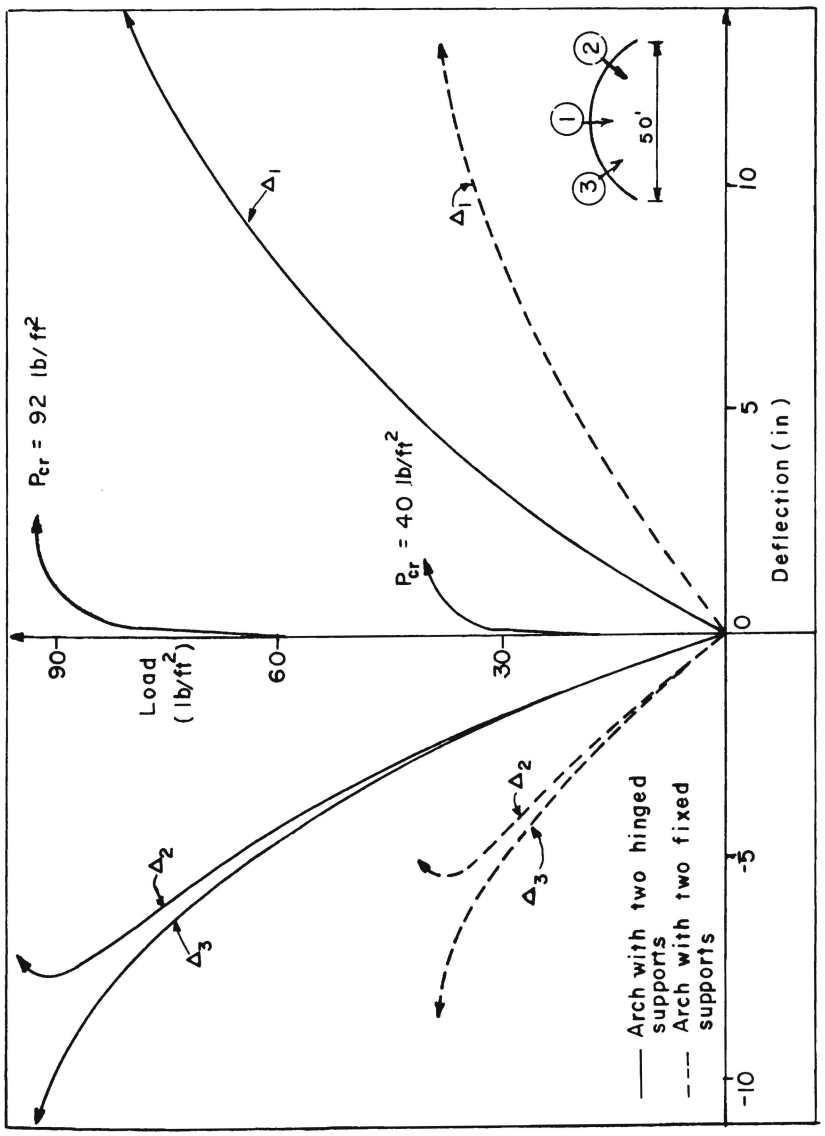

Fig. 9 Load vs. Deflection for Arch Considering Supports to be Fully Fixed or Hinged

[S = 50 ft (15.24 m), R = 310 in (79 m), ϕ_e = 75.1°, t = 0.03 in (0.76 mm)]

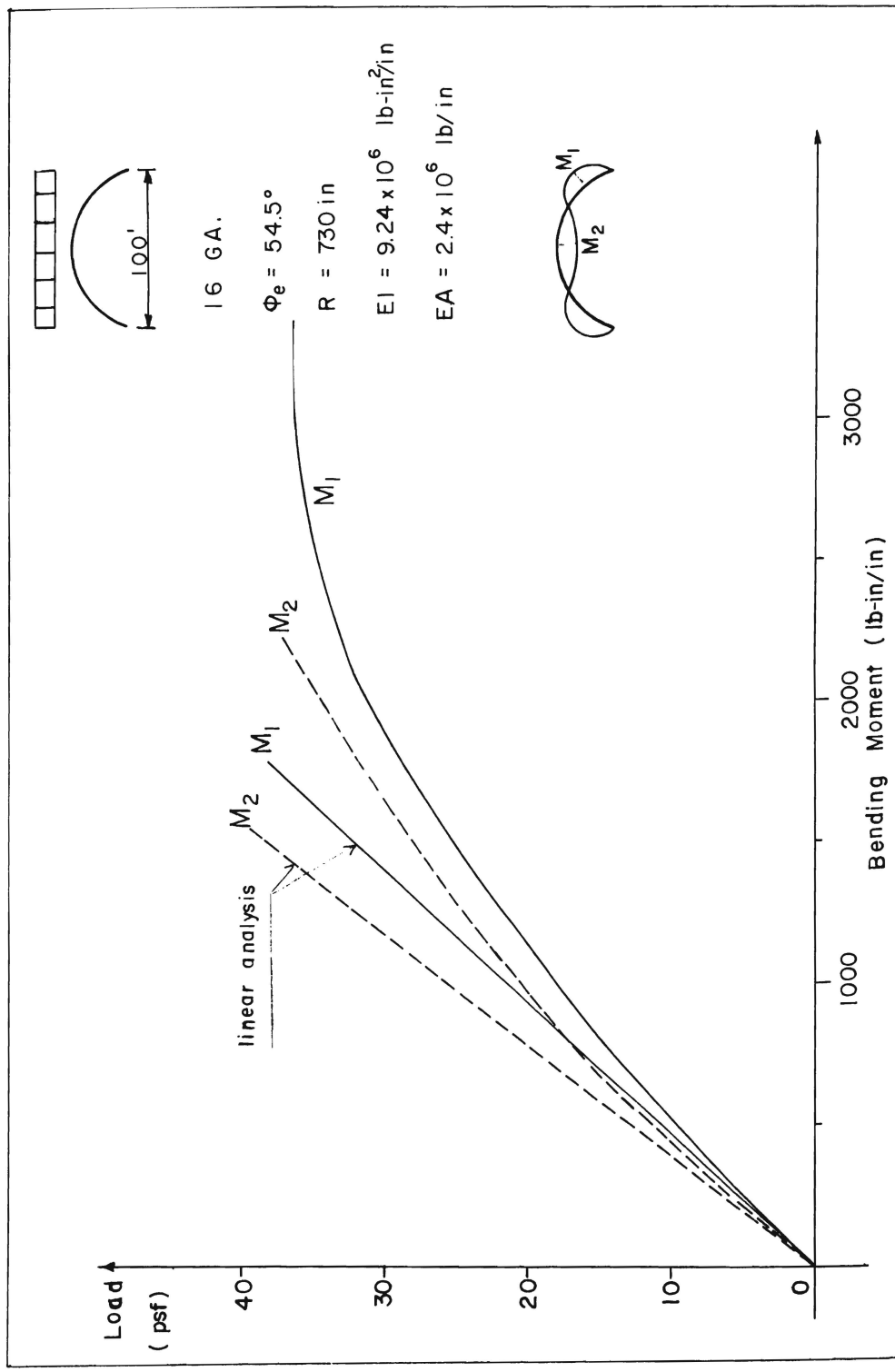

Fig. 10 Load vs. Bending Moment M_ϕ, Two Hinged Arch [S = 100 ft (30.48 m), R = 730 in (185.42 m), ϕ_e = 54.5°, t = 0.06 in (1.52 mm)]

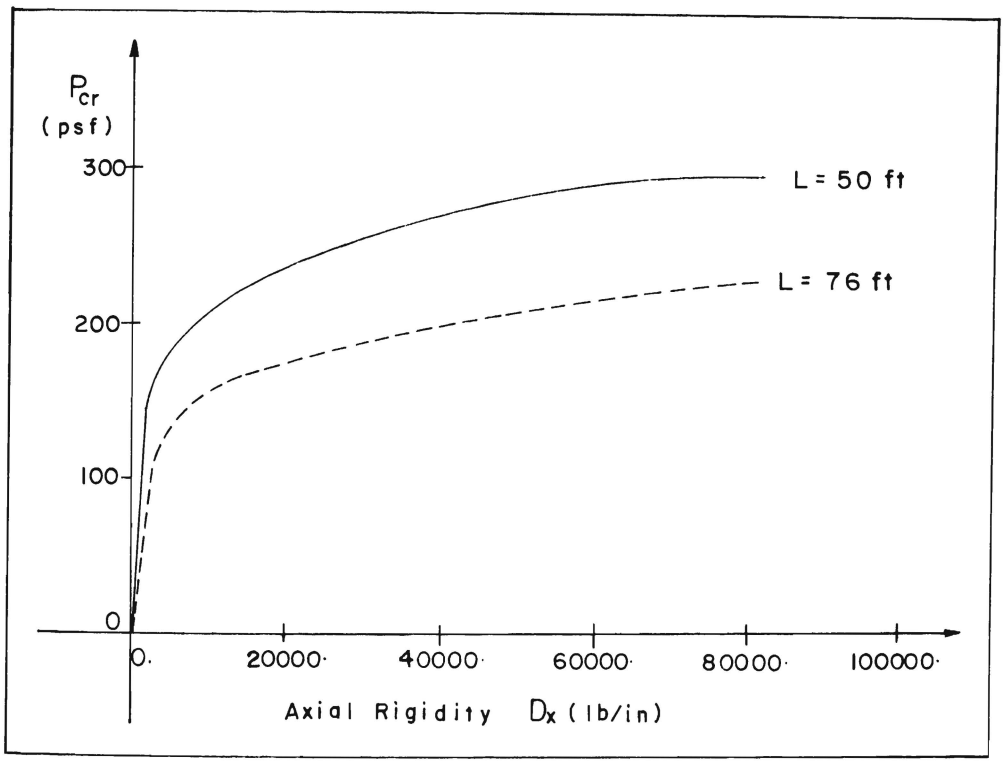

Fig. 11 Buckling Uniform Load on the Horizontal Projection vs. Axial Rigidity D_x [S = 50 ft (15.24 m), R = 310 in (79 m), ϕ_e = 75.1°, t = 0.03 in (0.76 mm)]

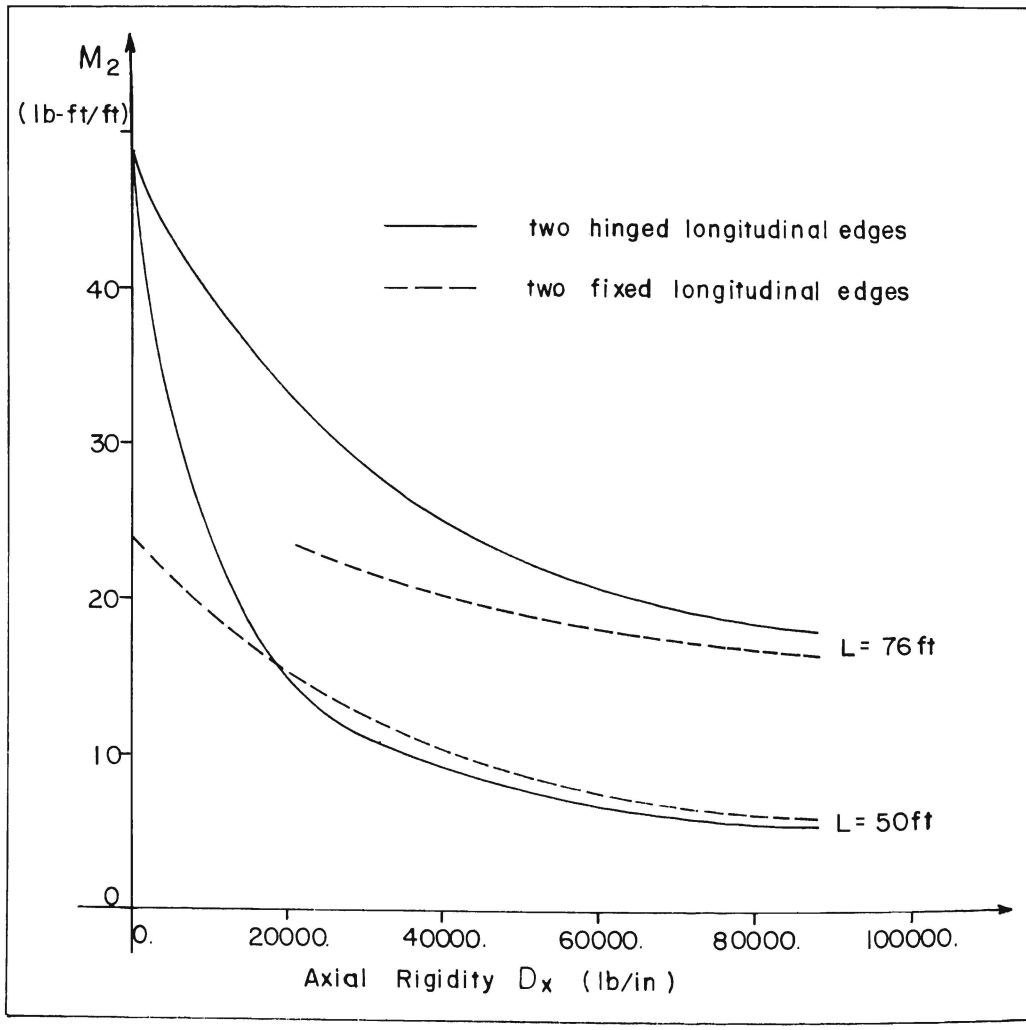

Fig. 12 Maximum Negative Moment vs. Axial Rigidity, D_x

[S = 50 ft (15.24 m), R = 310 in (79 m),
ϕ_e = 75.1°, t = 0.03 in (0.76 mm)]

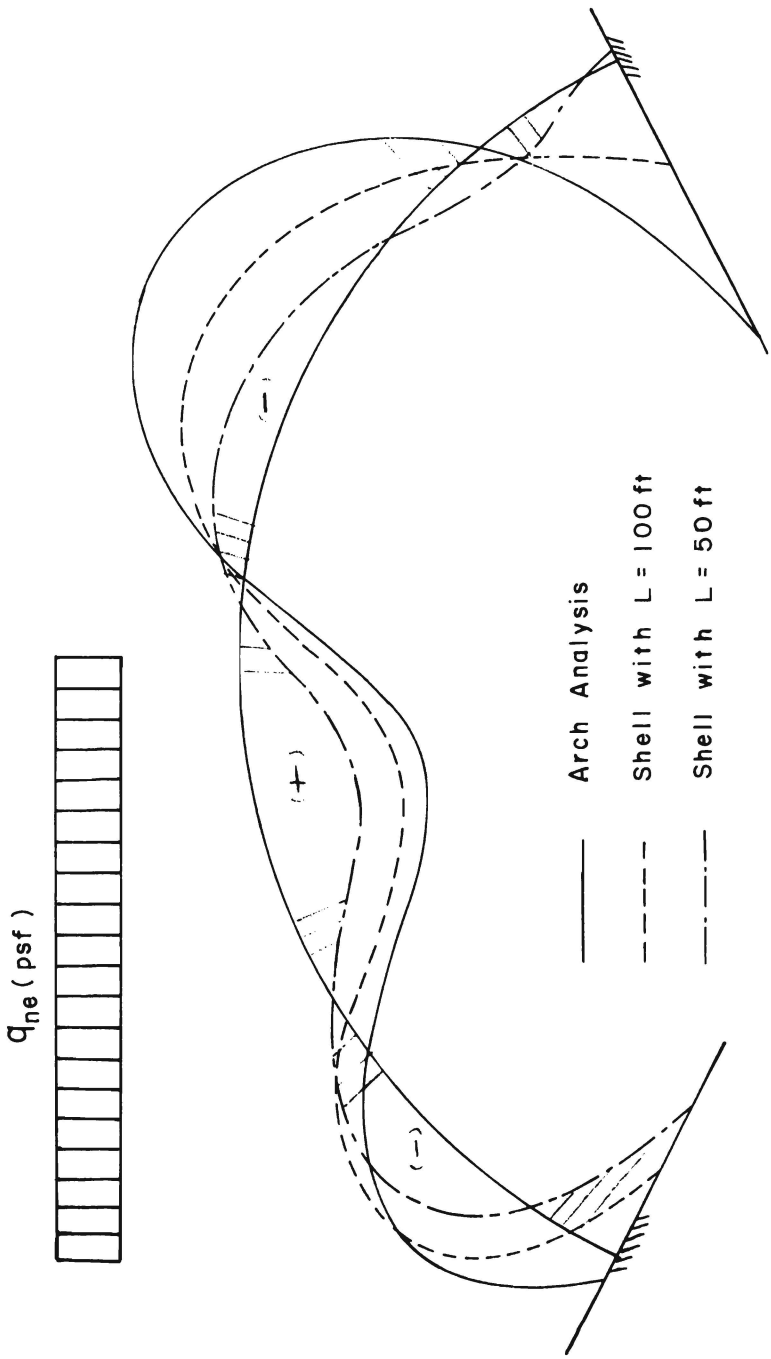

Fig. 13 Bending Moment Diagram for 1 psf (Scale: 1 cm = 10 lb. in/in)
[S = 50 ft (15.24 m), R = 310 in (79 m), ϕ_e = 75.1°, t = 0.03 in (0.76 mm)]